
**Liquid Crystals**
Publication details, including instructions for authors and subscription information:
http://www.informaworld.com/smpp/title~content=t713926090

# Synthesis and mesomorphic properties of new compounds exhibiting TGBA and TGBC liquid crystalline phases

Vladimíra Novotná[a]; Miroslav Kašpar[a]; Věra Hamplová[a]; Milada Glogarová[a]; Petra Bílková[a]; Valentina Domenici[b]; Damian Pociecha[c]
[a] Institute of Physics, Academy of Sciences of the Czech Republic, 182 21 Prague 8, Czech Republic [b] Dipartimento di Chimica e Chimica Industriale, Università degli studi di Pisa, 56126 Pisa, Italy [c] Laboratory of Dielectrics and Magnetics, Chemistry Department, Warsaw University, 02-089 Warsaw, Poland

**To cite this Article** Novotná, Vladimíra , Kašpar, Miroslav , Hamplová, Věra , Glogarová, Milada , Bílková, Petra , Domenici, Valentina and Pociecha, Damian(2008) 'Synthesis and mesomorphic properties of new compounds exhibiting TGBA and TGBC liquid crystalline phases', Liquid Crystals, 35: 3, 287 — 298
**To link to this Article: DOI:** 10.1080/02678290701862215
**URL:** http://dx.doi.org/10.1080/02678290701862215

*Liquid Crystals,*
Vol. 35, No. 3, March 2008, 287–298

Taylor & Francis
Taylor & Francis Group

# Synthesis and mesomorphic properties of new compounds exhibiting TGBA and TGBC liquid crystalline phases

Vladimíra Novotná[a]*, Miroslav Kašpar[a], Věra Hamplová[a], Milada Glogarová[a], Petra Bílková[a], Valentina Domenici[b] and Damian Pociecha[c]

[a]*Institute of Physics, Academy of Sciences of the Czech Republic, Na Slovance 2, 182 21 Prague 8, Czech Republic;* [b]*Dipartimento di Chimica e Chimica Industriale, Università degli studi di Pisa, via Risorgimento 35, 56126 Pisa, Italy;* [c]*Laboratory of Dielectrics and Magnetics, Chemistry Department, Warsaw University, Al. Zwirki i Wigury 101, 02-089 Warsaw, Poland*

*(Received 16 April 2007; in final form 5 December 2007)*

We synthesised a series of rod-like mesogens with a (S)-2-methylbutyl-(S)-lactate unit in the chiral chain that exhibited extremely wide temperature ranges in the TGBA and TGBC* phases. TGB phases were identified, based on typical textures in confined samples and in free-standing films, by Grandjean-Cano texture and by NMR studies on a deuterium-labelled isotopomer. A sufficiently high electric or magnetic field transformed the TGBA and TGBC* phases into their respective SmA and SmC* phases, the TGB structures being restored within some 20–30 minutes. Therefore values of the spontaneous polarisation and spontaneous tilt angle, when measured under a sufficiently high field, gave evidence of the properties of the SmC* phase. Temperature dependencies of relaxation frequency, dielectric strength, selective reflection and layer spacing showed anomalies at a certain temperature within the TGBC* phase range. Also, changes in textures, as well as in $^2$H-NMR spectra, occurred at this same temperature. These results suggest the existence of two TGBC* phases.

**Keywords:** lactate unit; the TGBA phase; the TGBC* phase; dielectric properties



## 1. Introduction

Twist grain boundary (TGB) phases that appear as an intermediate state between the cholesteric and smectic phase are examples of frustrated phases induced by molecular chirality. The analogy between smectics and superconductors was initially mentioned by de Gennes (*1*), while the TGB phases were theoretically described for the first time by Renn and Lubensky (*2–4*) and later discovered by the Bell Laboratories group (*5*). The TGBA phase has been confirmed as being organised in SmA blocks with their normal N rotated across each grain boundary by an angle $\Delta = 2\sin^{-1}(d/2l_d)$, where $d$ is the smectic period (layer spacing) and $l_d$ is the separation of parallel screw dislocation.

The reason for the TGB phase's appearance is that the direct cholesteric (Ch)-smectic phase transition cannot occur in a continuous way since the cholesteric twist of the director is not compatible with smectic layering. TGB phases exhibit distinct structural features: smectic layers and a helical superstructure with its axis parallel to the smectic layers. While the structure of the TGBA phase seems to be quite well understood, the character and properties of its tilted variants is still the subject of intense debate. The tilted TGBC phase was first experimentally proved by Nguyen and coworkers (*6*). Several types of TGBC phases with different local smectic structures have been described (*7–9*) and the phase transition between two TGBC phases found by calorimetric measurements (*8*). This variety arises from the differing organisation of the molecular tilt with respect to the plane of smectic layers and grain boundaries. Possible configurations of the tilted TGB phase have been analysed theoretically in (*2–4*) and two phases, designated as TGBC and TGBC*, have been proposed. In the TGBC phase molecular tilt in the smectic blocks is uniform, while in the TGBC* phase the blocks are filled by the SmC* phase modulated in a direction perpendicular to the block's normal. In (*10*) the Renn and Lubensky model was modified on the basis of the calculation of elastic interactions for the TGBC* phase. It has been suggested that the TGBC* phase could exist in several structural modifications – and transitions between different phases have been predicted (*10, 11*). Dielectric studies of TGB phases are scarce (*12–14*) and questions still exist concerning its temperature behaviour and the origin of observed modes. Ismaili et al. (*15*) have observed the soft mode in the TGBA phase and the Goldstone mode in the TGBC phase, the dielectric strength of both modes being much lower and relaxation frequency much higher compared to those found in the SmC* and SmA phases.

*Corresponding author. Email: novotna@fzu.cz

ISSN 0267-8292 print/ISSN 1366-5855 online

DOI: 10.1080/02678290701862215
http://www.informaworld.com

They explained this discrepancy on the basis of a modified Landau free energy, taking into account the elastic strain connected to the anchoring at the grain boundaries and the distance between them.

Liquid crystals incorporating lactate units frequently exhibit unusual mesomorphic properties, for example the presence of the re-entrant smectic C phase (*16–21*). However, the effect of the chiral centre number and/or its configuration (S, R) on the occurrence of mesophases has still not been clarified. Recently, mesogens with a naphthalene core and lactic unit in the chiral chain have been described that exhibit the TGBA phase (*21*). Nevertheless, the relationship between the structure and formation of the TGB phases is still unknown and their physical properties have not been systematically studied due to the rarity of these phases and their existence in such a narrow temperature interval. Here we report the synthesis and mesomorphic behaviour of a novel series of compounds with a three-benzene-ring core and (S)-2-methylbutyl-(S)-lactate unit in the chiral chain exhibiting TGBA and two different TGBC phases. Their physical properties are studied and discussed. One homologue was also prepared as a deuterated variant to enable $^2$H-NMR measurements.



## 2. Synthesis

General formula of the studied materials denoted as **HZLn/*** is in Scheme 1. The synthesis of the compounds studied was carried out according to the synthetic path described in Scheme 2. Both chiral centres have the (S) configuration.

The synthesis of chiral alcohol **1** has been described in detail in (*16*). As starting materials, we used commercial (S)-(-)-2-methylbutanol (Fluka), 99.5%, $[\alpha]^{20}_D = -6.3$, c=10 in ethanol and L-(+)-lactic acid (Fluka) ca. 80% solution in water and was prepared by fermentation containing less than 1% of D-antipod. After esterification we obtained (S)-(-)-2-methylbutyllactate with an optical rotation $[\alpha]^{20}_D = -11.1$ (neat). This is the same optical activity as described in (*16*).

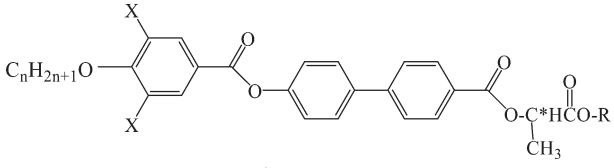


R = -$CH_2C^*H(CH_3)C_2H_5$

| | | |
|---|---|---|
| X = H | **HZLn/*** | n = 7, 8, 9 |
| X = D | **HZLn/*D** | n = 7 |

Scheme 1. Chemical formula of studied materials.

### 2.1. *Preparation of phenol 2*

Chiral alcohol **1** was esterified by protected 4-hydroxy-4′-biphenylcarbonyl chloride in a pyridine/dichloromethane mixture followed by ammonolysis in a chloroform/tetrahydrofurane mixture at 10°C. After separation of the reaction mixture by column chromatography on silica gel (using a mixture of dichloromethane and acetone 99:1 as the eluent), compound **2** was obtained in 50% yield.

$^1$H-NMR **2**, $CDCl_3$, 200 MHz

8.1d (2H, ortho to –COO); 7.58d (2H, meta to –COO); 7.42d (2H, meta to –OH); 6.90d (2H, ortho to –OH); 5.4q (1H, ArCOOCH*); 4.0m (2H, $COOCH_2$); 1.6d (3H, $\underline{CH}_3$, CHCOO); 1.2–1.7m (3H, CH-$CH_2$); 0.9m (6H, $CH_3$).

### 2.2. *Preparation of acids 3a and 3b*

Compound **3a** is commercially available. Deuterated acid **3b** is prepared by the following procedure: 4-hydroxybenzoic acid (4.0 g, 29.1 mmol) was dissolved in 50 g of 5% solution of deuterium chloride in $D_2O$. The solution was refluxed for 24 hours, then the mixture was cooled to 0°C and white solid powder was filtered and dried. A total of 3.4 g (yield 85%) of 4-hydroxy benzoic acid-$D_2$ was obtained.

$^1$H-NMR, DMSO-$d_6$, 200 MHz

12.4 (1H, broad s), 10.1 (1H, broad s), 7.7 (2H, s+very weak d), 6.8 (0.1H, d).

The esterification of the deuterated acid with heptylbromide was carried out by the usual method via the 4-hydroxybenzoic acid ($D_2$) ethylester, which was obtained by azeotropical esterification by ethylalcohol in toluene.

$^1$H-NMR, deuterated acid **3b**, $CDCl_3$, 200 MHz

8.1s (2H, ortho to –COO); 4.02t (2H, $CH_2OAr$); 1.8quint (2H, $\underline{CH_2}$ $CH_2OAr$); 1.3–1.7m (8H, $CH_2$); 0.9t (3H, $CH_3$).

From the $^1$H-NMR spectrum 95% deuteration was estimated.

### 2.3. *Preparation of final products*

The final products **HZLn/*** and **HZLn/*D** were prepared by standard methods of esterification with dicyclohexylcarbodiimid (DCC) in presence of dimethylaminopyridine (DMAP) in dichloromethane using acid **3a** and **3b**, respectively. Crude products were purified by column chromatography on silica gel using a mixture of dichloromethane and acetone (99.5:0.5) as an eluent and crystallised twice from a mixture of ethanol and acetone. The structure of all final products was confirmed by $^1$H-NMR (200 MHz, $CDCl_3$, Varian, Gemini 2000). The chemical purity of a compound was checked by high-performance liquid

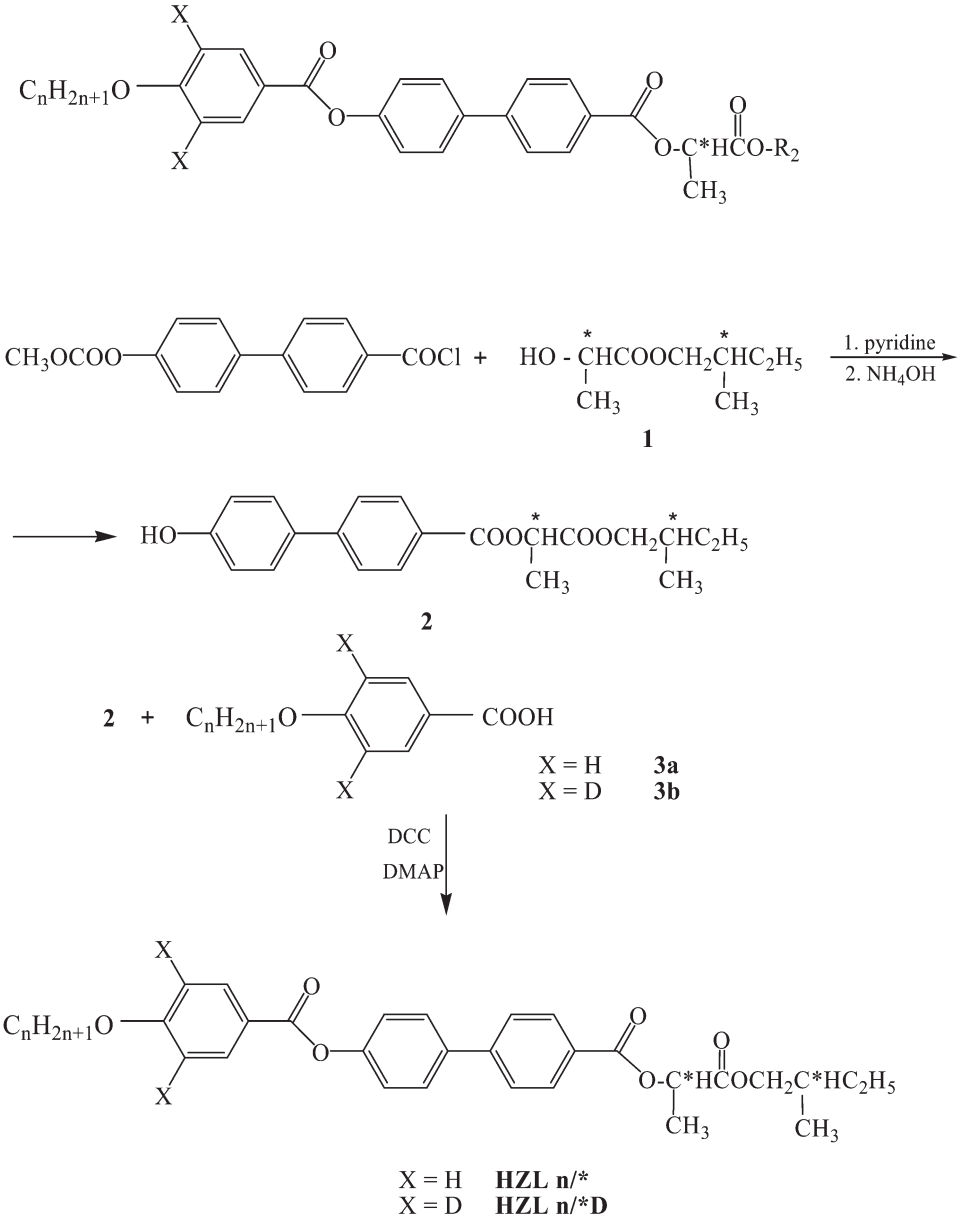


Scheme 2. Synthesis of studied compounds.

chromatography (HPLC), which was carried out with a Watrex HPLC chromatograph using a silica gel column (Biospher Si 5 µm, 4 × 250, Watrex) with a mixture of 99.9% of toluene and 0.1% of methanol as eluent, and detection of the eluting products by a UV-vis detector ($\lambda$=290 nm). Chemical purity was found to be better than 99.8% under these conditions.

$^1$H-NMR **HZL7/***, $CDCl_3$, 200 MHz

8.18d (4H, ortho to –COO); 7.68d (4H, ortho to –Ar); 7.30d (2H ortho to –OCO); 7.00d (2H, ortho to –OR); 5.40q (1H, CH*); 4.05m (4H, $CH_2OAr$ and $COOCH_2$); 1.7d (3H, $CH_3C$*); 1.2–1.9m (13H, CH+$CH_2$); 0.9m (9H, $CH_3$).

$^1$H-NMR **HZL7/*D**, $CDCl_3$, 200 MHz

8.18m (4H, ortho to –COO); 7.68m (4H, ortho to –Ar); 7.30d (2H ortho to –OCO); 5.40q (1H, CH*); 4.05m (4H, $CH_2OAr$ and $COOCH_2$); 1.7d (3H, $CH_3C$*); 1.2–1.9m (13H, CH+$CH_2$); 0.9m (9H, $CH_3$).

## 3. Experimental

The molecular structure of all synthesised compounds was checked using standard analytical methods. $^1$H-NMR spectra were acquired on a spectrometer Varian-Gemini 200 MHz, deuterochloroform, DMSO-$d_6$ serving as solvent and the signals of the solvent were used as internal standards. Chemical shifts are given in the $\delta$-scale (ppm), coupling

constant $J$(H,H) in Hz. IR spectra were recorded on a Nicolet FTIR 740 spectrometer in chloroform. Column chromatography was carried out at atmospheric pressure using silica gel (100–200 mesh, Merck).

Phase transition temperatures and enthalpies were determined by differential scanning calorimetry (DSC) studies (Pyris Diamond Perkin-Elmer 7) under cooling and heating runs at a rate of $5\,\mathrm{K\,min^{-1}}$. The samples of 2–5 mg were hermetically sealed in aluminium pans and placed in the calorimeter chamber inflated by nitrogen. The plane samples for texture observation and electric field studies were filled by capillarity action in the isotropic phase into cells composed of glasses with ITO transparent electrodes ($5\times5\,\mathrm{mm^2}$). The sample thickness was defined by mylar sheets. Cells with planar and homeotropic orientation and thickness 8 and 12 μm were used. For Grandjean–Cano textures (for details see (*22*)) the lower glass was covered with surfactant by spin-coating (ensuring planar anchoring) and rubbed on velvet. A lens with a large focal length was used as an upper glass cover. Free-standing films were spread over a circular hole (diameter 2 mm) in an aluminium plate. All texture observations were performed using a Nikon Eclipse polarising microscope equipped with a Linkam hot stage.

Spontaneous polarisation, $P_s$, was determined from hysteresis loops detected during switching at a frequency of 50 Hz and an electric field of about $40\,\mathrm{kV\,cm^{-1}}$. The spontaneous tilt angle, $\theta_S$, was determined from the angular difference between extinction positions after the helicoidal structure was unwound in opposite d.c. electric fields of about $\pm10\,\mathrm{kV\,cm^{-1}}$.

Frequency dispersion of dielectric permittivity was measured on cooling using a Schlumberger 1260 impedance analyser in a frequency range of 1 Hz–1 MHz, keeping the temperature of the sample stable during frequency sweeps within $\pm0.1$ K. The frequency dispersion data were analysed using the Cole–Cole formula (*14*) for the frequency dependent complex permittivity complemented by second and third terms to eliminate the low frequency contribution from d.c. conductivity $\sigma$ and the high-frequency contribution due to resistance of the ITO electrodes, respectively:

$$\varepsilon^* - \varepsilon_\infty = \frac{\Delta\varepsilon}{1+(if/f_r)^{(1-\alpha)}} - i\frac{\sigma}{2\pi\varepsilon_0 f^n} + Af^m \qquad (1)$$

where $f_r$ is the relaxation frequency, $\Delta\varepsilon$ the dielectric strength, $\alpha$ the distribution parameter of relaxation, $\varepsilon_0$ the permittivity of a vacuum, $\varepsilon_\infty$ the high-frequency permittivity and $n$, $m$, $A$ are parameters of fitting. Measured real, $\varepsilon'$, and imaginary, $\varepsilon''$, parts of dielectric permittivity $\varepsilon^*(f)=\varepsilon'-i\varepsilon''$ were simultaneously fitted to formula (1).

The selective reflection measurements were performed in transmission mode at normal incidence with a Shimadzu PC3101 spectrophotometer for free-standing film samples in the wavelength range 250–3200 nm. At normal incidence the selective reflection from the half-pitch band was detected and a mean refractive index of $n=1.5$, that is assumed to be temperature independent within the temperature range of measurements, was used for calculating the pitch length. The smectic layer thickness was measured by X-ray diffraction from one surface free samples (which assured homeotropic alignment) using a modified DRON system (Graphite monochromator, CuK$\alpha$ line) working in reflection mode.

$^2$H-NMR experiments were performed by using a Varian Infinity Plus 400 double channel spectrometer operating at the deuterium frequency of 61.39 MHz (9.4 T), equipped with a goniometric probe for recording static spectra. These spectra were acquired by using the quadrupolar echo sequence (*23–24*) with a 90° pulse of 4.6 μs, a pulse delay of 0.5 s, a quadrupolar echo delay ($\tau$) of 30 μs and 400 scans. The sample was aligned within the magnet by slow cooling from the isotropic phase. The temperature was stable within 0.2°C. The spectra recorded in the lower magnetic field (4.7 T) were measured by a 200 VXL Varian double channel spectrometer operating at the deuterium frequency of 30.7 MHz, using a standard 5 mm probe for liquid samples. A single pulse sequence with a rectangular pulse of 12 μs, a pulse delay of 0.8 s and 200 scans was used.

## 4. Results

All studied compounds exhibited the same phase sequence, namely isotropic–cholesteric–TGBA–TGBC* on cooling. The justification for the identification of phases is given below. The phase transition temperatures and enthalpies were determined from DSC studies and are summarised in Table 1. All DSC data were taken at a rate of $5\,\mathrm{K\,min^{-1}}$ within the temperature range of −25°C to 150°C. Crystallisation usually took place at temperatures below room temperature, and for **HZL8/*** and **HZL9/*** no crystallisation occurred even on cooling down to −25°C. For such compounds the crystallisation process started on heating, which was manifested on the DSC plots as an opposite peak. For **HZL8/*** the DSC plot is shown in Figure 1, where the profile of the peak connected with the TGBA–TGBC* transition is shown at an enlarged scale.

Table 1. Melting point, m.p., was indicated on third heating from −25°C, phase transition temperatures, $T_{tr}$, in °C and corresponding enthalpies, $\Delta H$, detected on second cooling and presented in square brackets in kJ mol$^{-1}$, and $n$ denotes the alkyl chain length; see Scheme 1. Star indicates that the phase transition was not recognisable in the DSC plots and was determined from texture studies.

| | $n$ | m.p. [$\Delta H$] | $TGBC_2$* | $T_{tr}$ [$\Delta H$] | $TGBC_1$* | $T_{tr}$ [$\Delta H$] | TGBA | $T_{tr}$ [$\Delta H$] | Ch | $T_{tr}$ [$\Delta H$] | Iso |
|---|---|---|---|---|---|---|---|---|---|---|---|
| **HZL7/*** | 7 | 67 [+17.4] | • | 70 [*] | • | 86 [−0.24] | • | 120 [−0.80] | • | 123 [−1.32] | • |
| **HZL7/*D** | 7 | 67 [+14.8] | • | 71 [*] | • | 87 [−0.27] | • | 118 [−0.46] | • | 122 [−1.09] | • |
| **HZL8/*** | 8 | 49 [+6.5] | • | 80 [*] | • | 93 [−0.16] | • | 120 [−1.41] | • | 122 [−1.47] | • |
| **HZL9/*** | 9 | 66 [+24.4] | • | 79 [*] | • | 96 [−0.42] | • | 111 [−0.78] | • | 120 [−1.26] | • |

In the next paragraphs we suggest the existence of two different TGBC* phases and designate them as $TGBC_1$* and $TGBC_2$* phase on subsequent cooling. The phase transition between them (see Table 1) is identified from microscopic observations as a change of texture and sample colour.

### 4.1. *Texture observations*

Under homeotropic boundary conditions the so-called filament texture was observed (see Figure 2 for **HZL7/*D**), similar to that described in (*21*). In the TGBA phase, bright coloured filaments are visible in a non-birefringent background (Figure 2 (a)). In the $TGBC_1$* phase the birefringence (double refraction) appeared (Figure 2 (b)) and the colour changed discontinuously at the $TGBC_1$*–$TGBC_2$* phase transition (compare Figures 2 (c) and 2 (d)).

The free-standing textures are shown in Figure 3. In the TGBA phase, a filament texture was observed (Figures 3 (a) and (b)), the amount of filaments increasing on heating and the pseudo-fan type of texture appearing in the close vicinity of the transition into the cholesteric phase (Figure 3 (c)). No filaments survived in the TGBC* phase on cooling – only a schlieren texture was seen. This fact could be explained by the unwinding of the TGBC* superstructure due to the effect of free surfaces. A change of colour at the $TGBC_1$*–$TGBC_2$* phase transition took place, similar to that in the homeotropic sample (see Figures 2 (c) and (d)).

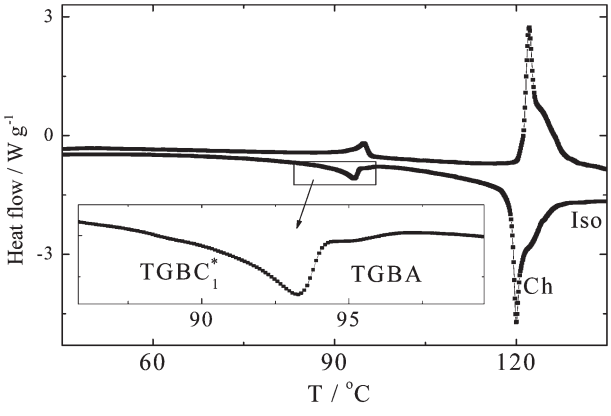


Figure 1. DSC plots for compound **HZL8/***. The upper and lower curves show the second heating from RT and subsequent cooling runs, respectively. In the inset, cooling in the vicinity of the TGBA–$TGBC_1$* phase transition is enlarged.

In the cell with planar boundary conditions, typical oily-streaky textures were observed in the cholesteric phase, which very often survived deep into the temperature range of the TGBA phase. The coloured pseudo-fan texture, which could not be focused (see Figure 4 (a)), was characteristic for planar geometry in the TGBA phase (*22*). On cooling, the TGBA–TGBC* phase transition was observed as an abrupt sharpening of contrast and change of fan colour (see Figure 4 (b)). A continuous sharpening of fans took place within the TGBC* phase temperature range. The $TGBC_1$*–$TGBC_2$* phase transition was not exactly visible in contrast to the homeotropic sample, but, below this temperature, evolution of the texture, as well as the changes of colour, were more pronounced (Figure 4 (c)). On applying an electric field in the TGBA phase, the texture started to become even more blurred. On approaching the TGBA–TGBC* phase transition, the application of an electric field higher than 1 V μm$^{-1}$ led to a gradual transformation into the regular fan-shaped texture, typical for the SmA phase (dark fans in extinction were already transformed to the SmA phase in Figure 4 (d)). Within the whole temperature range of the TGBC* phases, the application of an electric field led to a complete transformation into the regular broken fan-shape SmC* texture. The helix of the SmC* structure was probably unwound because of the field. We suppose that after switching the field off, the helical structure of the SmC* phase was quickly restored, even though no dechiralisation lines were visible in the temperature range of the $TGBC_1$* phase (see Figure 4 (e)). This fact might be explained by the short helical pitch below 1 μm. The lines became visible under the low electric field, which increased the pitch but did not unwind the helix completely. In the temperature range of the $TGBC_2$* phase, the dechiralisation lines

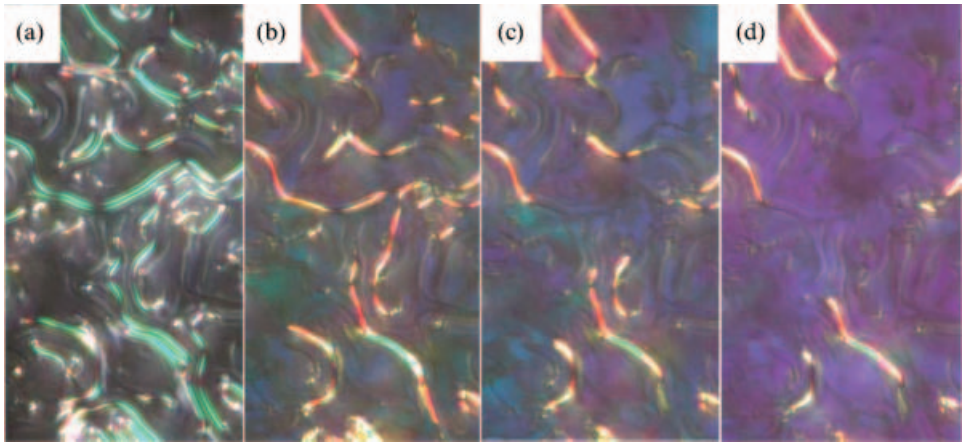


Figure 2. Textures of **HZL7/*D** under homeotropic boundary conditions detected on cooling: (a) TGBA phase at $T=89^{\circ}$C, (b) TGBC$_1$* phase at $T=77^{\circ}$C, (c) TGBC$_1$* phase at $T=71^{\circ}$C and (d) TGBC$_2$* phase at $T=70^{\circ}$C. The width of every photo is about 120 µm.



appeared just after the field was switched off, showing a significantly longer helical pitch (Figure 4 (f)). The lines disappeared gradually while the reconstruction of the typical TGBC$_2$* texture proceeded. Complete restoring of the TGBC$_1$* phase was accomplished within at least 20 minutes after the electric field had been switched off; for the TGBC$_2$* phase this process was considerably slower.

One of the most typical textures of the TGB phase were the so-called Grandjean–Cano textures, with defect lines separating the zones where the number of helix turns differed by 1/2 or a multiple of this value (*22*). We obtained typical Grandjean–Cano textures in the TGBA phase several degrees above the TGBA–TGBC$_1$* phase transition. The TGBA–TGBC$_1$* phase transition was clearly demonstrated by the phase frontier seen as a step change of colour (see Figure 5 for **HZL7/*D**). No visible discontinuity in colour was observed in the Grandjean–Cano textures at the TGBC$_1$*–TGBC$_2$* phase transition.

### 4.2. *Spontaneous polarisation and tilt angle in the TGBC* phases*

We measured the spontaneous polarisation, $P_s$, and the spontaneous tilt angle, $\Theta_s$, for all studied compounds. The values of spontaneous polarisation exhibited no saturation tendency down to low temperatures except for **HZL9/*** and reached large values up to 190–270 nC cm$^{-2}$ depending on the material (see Figure 6 (a)). For all compounds, spontaneous tilt angles reached up to 35–38° at saturation (see Figure 6 (b)). As the coercive field strongly increased below 40°C, we were not able to measure it for lower temperatures. In the TGBA phase on approaching the TGBA–TGBC$_1$* phase transition on cooling, tilt values significantly depended on the strength of the electric field, illustrating a strong electroclinic effect. At the TGBC$_1$*→TGBC$_2$* phase transition, no anomalies were detected on $P_s(T)$ and $\Theta_s(T)$ dependence (see Figures 6 (a) and 6 (b), respectively). Both quantities were measured under a

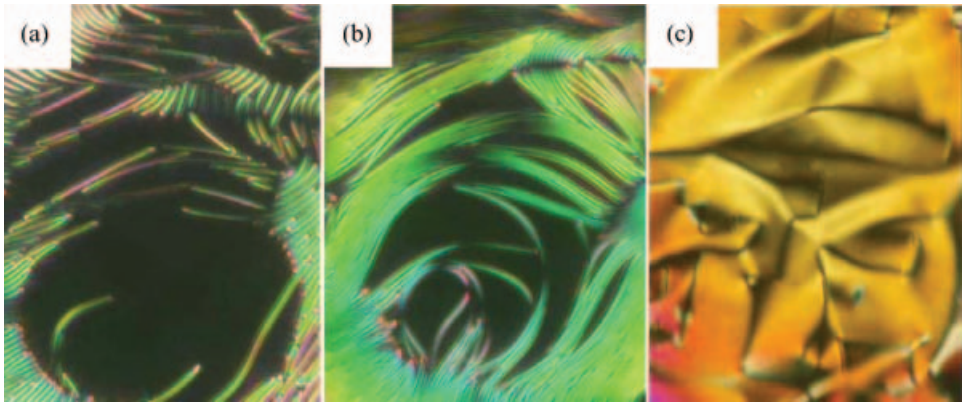


Figure 3. Texture of free-standing film of **HZL7/*** in the TGBA phase at temperatures of about (a) $T=115^{\circ}$C and (b) $T=118^{\circ}$C, (c) $T=119^{\circ}$C, in the vicinity of the TGBA–Ch phase transition. The width of each figure is about 250 µm.

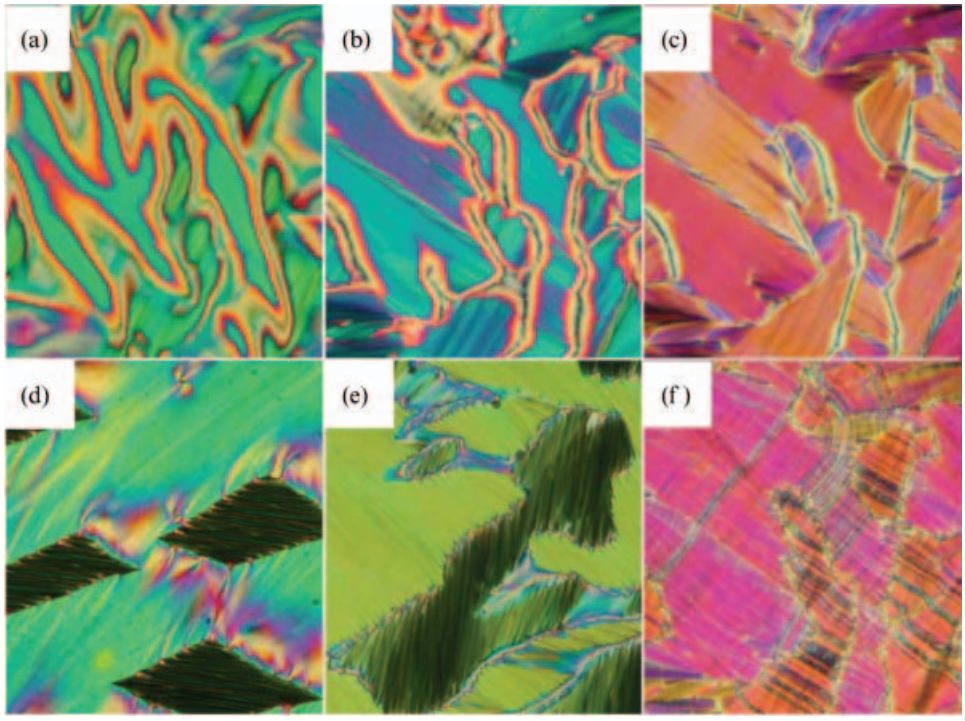


Figure 4. Planar texture of **HZL7/*** obtained on cooling from the isotropic phase: (a) TGBA phase at $T=85^{\circ}C$, (b) $TGBC_1$* at $T=76^{\circ}C$; and (c) $TGBC_2$* at $T=70^{\circ}C$, (d) TGBA phase at $T=87^{\circ}C$ under an a.c. electric field, dark areas were already in the SmA phase; (e) and (f) were textures after the applied electric field was switched off: (e) $T=76^{\circ}C$, the $TGBC_1$* has started to reappear (the blue areas) in the SmC* texture induced by the field, (f) $T=70^{\circ}C$, the field induced SmC* phase existed in blocks bounded by defects. The width of figures (a)–(c) corresponds to 200 µm, that of (d)–(f) to 100 µm.



sufficiently high electric field for the TGBC* phase to be transformed to the regular SmC* phase. Thus both $P_s$ and $\Theta_s$ values were not experimentally accessible in the TGBC* phase.

### 4.3. *Dielectric spectroscopy*

The frequency dispersion of complex permittivity was measured at stabilised temperatures over a wide range of temperatures of the TGBA and TGBC*

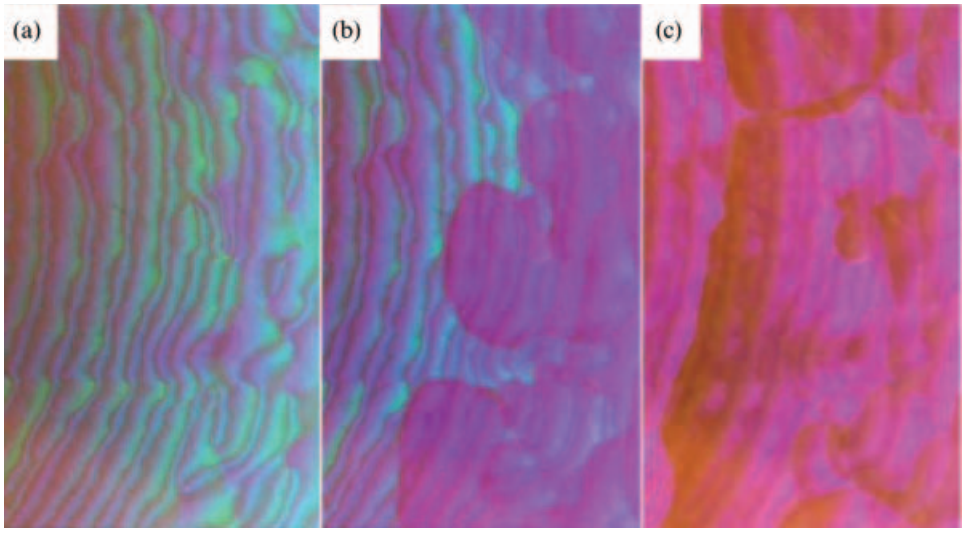


Figure 5. Grandjean–Cano textures of **HZL7/*D** subjected to the planar boundary condition (a) $T=91^{\circ}C$ (in the TGBA phase), (b) TGBA–$TGBC_1$* phase transition, (c) $T=75^{\circ}C$ (in the $TGBC_1$* phase). The width of figures corresponds to about 150 µm.

phases. A 3D plot of the imaginary part of dielectric permittivity versus temperature in the frequency range 10 Hz–1 MHz is shown in Figure 7 for the compound **HZL7/***. In the studied frequency range one mode was detected and fitted, thus obtaining the temperature dependence of its dielectric strength, $\Delta\varepsilon$(T), and relaxation frequency, $f_r(T)$. For **HZL9/***, temperature profiles of $\Delta\varepsilon$(T) and $f_r(T)$ are shown in Figure 8. On cooling from the TGBA phase, $\Delta\varepsilon$ increased at the TGBA–TGBC$_1$* phase transition and reached relatively high values. The relaxation process in the TGBA phase can be attributed to the amplitude fluctuation of the molecular director, the so-called soft mode, which may exist in small blocks of the TGBA phase similar to how it exists in the SmA phase. For all studied compounds, a softening of this mode was found (linear dependence of the fitted relaxation frequency in the temperature range 10 K above the TGBA–TGBC* phase transition). Below the TGBA phase, the detected mode could be ascribed to the Goldstone mode. Nevertheless, relaxation frequency having such a strong temperature dependence was not typical for the Goldstone mode in the SmC* phase. The soft mode in the TGBC* phase was overwhelmed by the strong Goldstone mode.

For all studied compounds, a pronounced anomaly in dielectric permittivity was found at a certain temperature within the temperature range of the TGBC* phase. In Figure 7 for **HZL7/***, such an anomaly is marked by an arrow. For **HZL9/***, we measured several planar samples with different thicknesses (12, 25 and 7 µm). Independent of surface treatment and thickness, we found an anomaly in $\Delta\varepsilon$(T) and $f_r(T)$ in the form of a change of slope in $f_r(T)$ as well as $\Delta\varepsilon$(T) (see Figure 8). We suppose this anomaly was connected with the TGBC$_1$*→TGBC$_2$* phase transition.

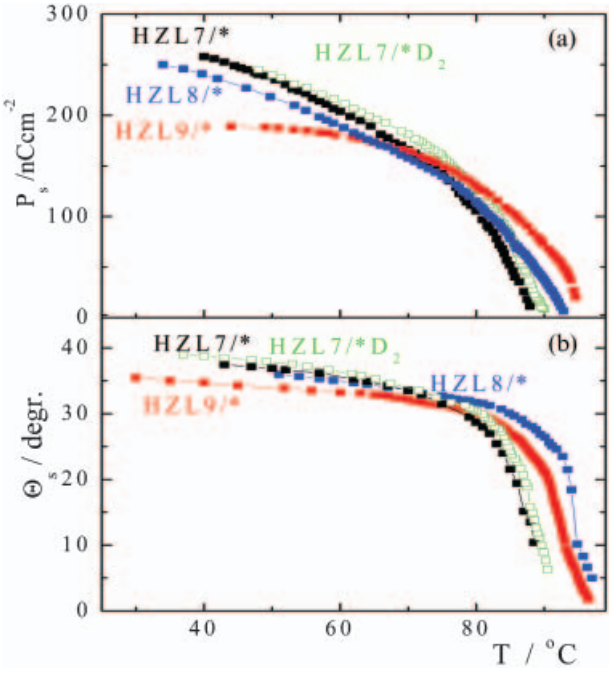


Figure 6. Temperature dependencies of (a) spontaneous polarisation, $P_s$, and (b) spontaneous tilt angle, $\Theta_s$, for all studied compounds.

In the TGBC* phases, the application of a biased electric field led to a suppression of the relaxation process, which could be explained by a transformation to the SmC* phase with the unwound helix (see section 4.1). After the electric field was switched off, first a pronounced increase of $\Delta\varepsilon$ and decrease of $f_r$ occurred, reaching much higher and lower respective values than in the TGBC* phase. These values corresponded to the helical SmC* phase and relaxed slowly to the TGBC* values.

### 4.4. *X-ray study and selective reflection measurements*

From X-ray diffraction measured at a range of small scattering angles, the layer spacing $d$ was evaluated (see Figure 9). In the TGBA phase, a slight increase of $d$ was seen on cooling, similar to the behaviour in the SmA phase. Such an increase used to be explained by an increase of long molecular axis ordering (*23*). At the TGBA–TGBC$_1$* phase transition, $d(T)$ clearly showed a decrease, which reflected the tilt of molecules. Another jump-like decrease was found at the temperature corresponding to the anomaly in $\Delta\varepsilon$(T) (see Figures 7 and 8). We attribute this anomaly to the TGBC$_1$*–TGBC$_2$* transition. The existence of this transition is supported by selective reflection measurements performed in transmission mode for free-standing films in the wavelength range 250–3200 nm. At normal incidence, the selective reflection (SR) was observed and temperature dependence of the corresponding wavelength exhibited a decline at the TGBC$_1$*–TGBC$_2$* phase transition (see Figure 9). In addition, the shape of the SR signal and the character of the background also changed at this transition, the signal becoming much broader.

### 4.5. *$^2$H-NMR studies*

The deuterium-labelled compound **HZL7/*D** (Scheme 1, Table 1) was used to perform $^2$H-NMR investigations. The presence of deuterons allowed us to obtain quite simple $^2$H-NMR spectra. In principle, the use of $^2$H-NMR spectroscopy was the best way to study the orientational and dynamic properties, as well as the molecular structure (*24–31*). In our

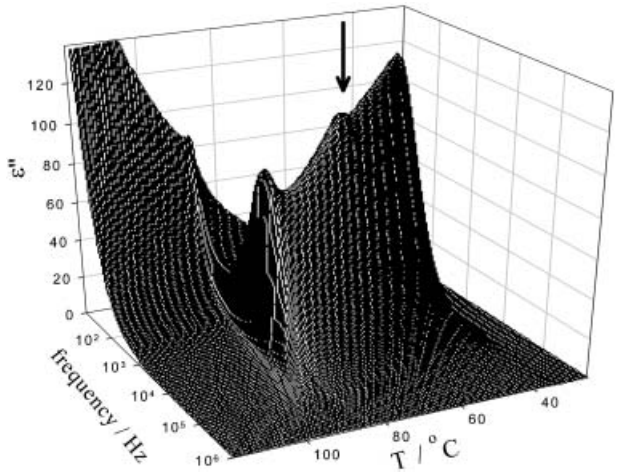


Figure 7. Temperature–frequency plots of the imaginary part of dielectric permittivity taken on cooling from the isotropic phase for **HZL7/***. An arrow marks the anomaly at the $TGBC_1$*–$TGBC_2$* phase transition.

measurements, the aim was to check the mesogenic properties and to get qualitative information about the character of the mesophase. The main features of the spectra recorded in a high magnetic field (9.4 T) were the simplicity of the spectrum and the clear transition from an untilted phase to a tilted phase at about 87°C (see Figure 10). The $^2$H-NMR spectra, acquired using a quadrupolar echo sequence under proton decoupling, were characterised by a single quadrupolar doublet, which we could ascribe to the aromatic deuterons.

In the TGBA phase, quadrupolar splitting grew on cooling due to the increase in the orientational order, *S*. At the TGBA–$TGBC_1$* phase transition, a big jump down in the quadrupolar splitting was observed and at lower temperatures the quadrupolar splitting continued to decrease. This tendency

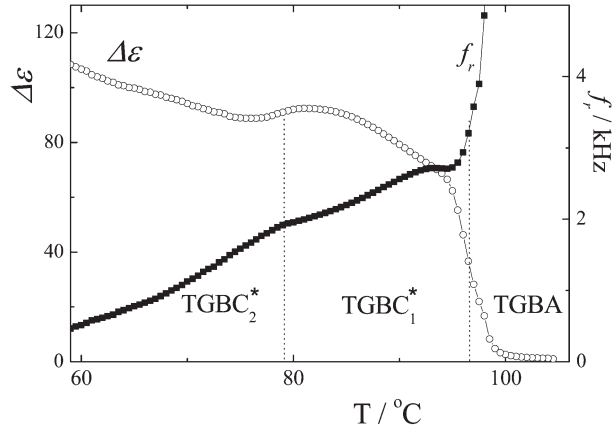


Figure 8. Temperature dependencies of relaxation frequency, $f_r$, and dielectric strength, $\Delta\varepsilon$, for **HZL9/*** (12 μm thick planar sample).

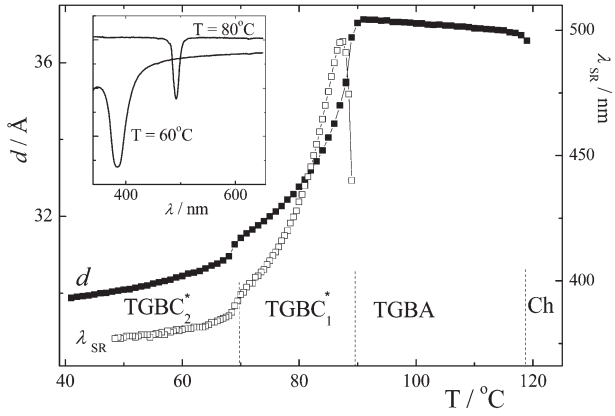


Figure 9. Temperature dependence of layer spacing and selective reflection wavelength for **HZL7/***. In the inset are examples of profiles of intensity of transmitted light dependent on wavelength in the $TGBC_1$* ($T$=80°C) and $TGBC_2$* phases ($T$=60°C).

persisted throughout the whole temperature range of the TGBC* phase. Moreover, the $^2$H-NMR line-width progressively increased, giving rise to much broader signals, as observed in the chiral smectic C* phase (*26–31*). The decrease in the quadrupolar splitting and the increase of the line-width on cooling the sample were indeed typical for the tilted phases, due to the scaling of the order parameter *S* by a factor proportional to $(3(\cos\theta(T))^2-1)$, where $\theta(T)$

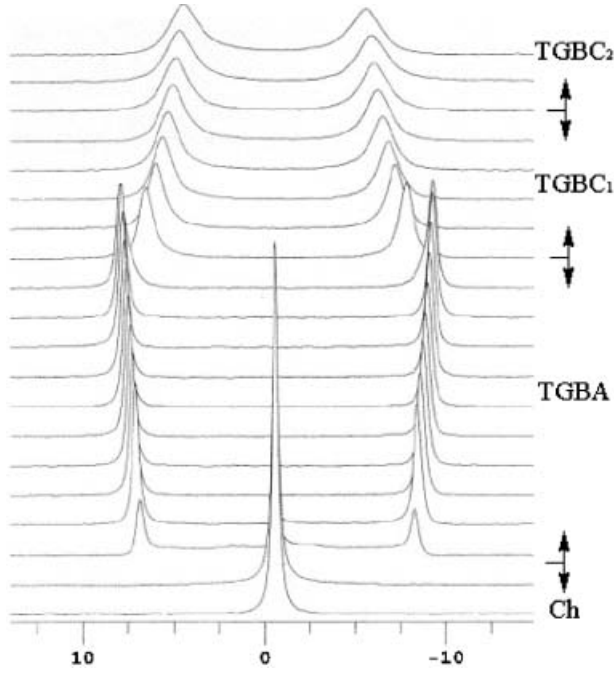


Figure 10. $^2$H-NMR spectra for **HZL7/*D** recorded at 9.40 Tesla, by cooling the sample from the isotropic phase. A series of spectra acquired by proton decoupling from 123°C to 66°C every 3 degrees. Phase ranges shown at the right are taken from Table 1.

was the tilt angle, and to changes in the dynamic processes.

The simple features of the recorded spectra in a magnetic field of 9.4 T were consistent with a molecular system uniformly oriented in a magnetic field, with the local director *n* oriented in the preferred direction with respect to the external magnetic field. No distributions of directors were present in this case, meaning that the supramolecular structure typical of the TGB phase was here destroyed by the magnetic field. In fact, the $^2$H-NMR spectra of liquid crystals showing the TGBA phase, with a magnetic susceptibility $\Delta\chi<0$ as is typical of calamitic liquid crystals, were characterised by a 'powder pattern' due to the cylindrical distribution of directors, as reported in (*26*) and (*27*). On the other hand, this was not the first case of a strong effect of a magnetic field over the mesophase structure of frustrated mesophases. It has been found for instance as an unwinding of the helical superstructure in the ferroelectric SmC* phase by a magnetic field (*26*) or as the effect of a magnetic field on the $^2$H-NMR line-shape of re-entrant smectic phases (*31*).

The $^2$H-NMR investigations were performed at a lower magnetic field, namely 4.7 Tesla. This field was not so high so as to destroy the TGB structure. A selection of $^2$H-NMR spectra recorded without proton decoupling by cooling the sample from the isotropic phase to the crystalline one is depicted in Figure 11. At the phase transition between the cholesteric and the TGBA phase, a sudden broadening of the signal started to retain the spectral features typical for the cholesteric phase, as shown in Figure 11 (a). This fact strongly confirms the TGBA character of the studied phase. Below 87°C, the $^2$H-NMR spectra drastically changed. The appearance of a different distributed spectrum meant that in this magnetic field the supramolecular structure of the TGBC* phase is neither unwound nor destroyed. The line-shape changes at about 70°C, which fits the value of the $TGBC_1$*–$TGBC_2$* phase transition temperature proposed from previous experiments.

The analysis of the $^2$H-NMR spectra recorded in the two magnetic fields – in terms of orientational order and other structural properties – is in progress (*32*). Preliminary $^{13}$C-NMR investigations have confirmed our findings about the effect of a magnetic field on the TGB structures.

## 5. Discussion and conclusions

This paper has reported a series of new compounds, exhibiting an extremely wide temperature range of TGBA and tilted TGBC* phases. The existence of these frustrated phases probably originated from the nature of the molecular chiral chain possessing two chiral centres (*9*).

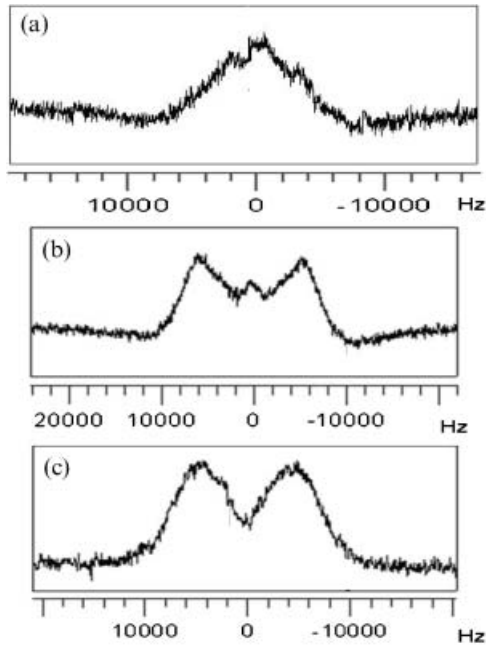


Figure 11. Selection of $^2$H-NMR spectra recorded at 4.70 Tesla on cooling from the isotropic phase without proton decoupling for **HZL7/*D**. Spectrum in (a) the TGBA phase (105°C), (b) the $TGBC_1$* phase (75°C) and (c) the $TGBC_2$* phase (65°C).

The existence of TGB phases in the studied compounds was confirmed by the typical textures in planar samples as well as in free-standing films and by the Grandjean–Cano textures in wedge-shaped samples. The NMR study performed in a lower magnetic field confirmed also the TGB character of the phases occurring below the cholesteric phase. Both TGBA and TGBC* phases are transformed to the respective SmA and unwound SmC* phases under a sufficiently high electric or magnetic field. For an electric field, it was shown that when the field was switched off the SmC* phase was quickly wound with a very short helical pitch, while the TGB structure was not restored for another 20 minutes. The effect of the electric-field-induced phase transition from TGBA and TGBC* to SmA and SmC* phases has already been described in (*33*).

The measurement of the layer spacing, *d*, accomplished on cooling by means of X-ray diffraction, showed *d* very slightly increasing within the TGBA phase similar to that which is typical for the SmA phase, where it used to be explained as an increase of ordering of the molecular long axes (*23*). Under a high magnetic field, such ordering has been found in NMR studies within the temperature range of the

TGB phase (see section 4.5). When entering the TGBC* phase, a strong decrease of *d* occurred, confirming the tilt of molecules within the smectic layers.

Dielectric spectroscopy threw some light on the modes existing in the TGB phases. Similar to that seen in the classical SmA and SmC* phases, the mode found in the TGBA phase could be attributed to the soft mode, while in the TGBC* phase only the Goldstone mode was visible, the soft mode being too weak. These modes were reduced due to the elastic strain originating in the anchoring of molecules at the grain boundaries (*15*). This effect could explain the observed relatively low dielectric strengths and high increase of relaxation frequencies compared to those usually found in the classical SmA and SmC* phases.

The following are quoted experimental results suggesting the existence of a phase transition between two possible TGBC* phases: a sharp change of texture colour was observed in homeotropic samples and free-standing films. The temperature of this change is taken as the transition temperature between two TGBC* phases (see Table 1). An anomaly at the same temperature is also seen in the dielectric properties, namely in the imaginary part of permittivity (Figure 7), the dielectric strength and relaxation frequency of the Goldstone mode (Figure 8), and further in the layer spacing and selective reflection (Figure 9). As the transition between the TGBC* phases can be only of the first order (*11*), the anomalies may be smeared due to the coexistence of phases. A difference was also seen between the line-shape of the $^{2}$H-NMR spectra recorded in a low magnetic field in each TGBC* phase (see Figure 11). The $^{2}$H-NMR line-shape of these spectra was quite complex. Analysis of the spectra showed that the molecules were tilted and organised in helicoidal structures, so that the phases were really TGBC* and not TGBC. Further investigations based on $^{2}$H- and $^{13}$C-NMR measurements in different magnetic fields are in progress in order to clarify the structure of all TGB mesophases. One cannot find this transition between the two TGBC* phases in the temperature dependencies of spontaneous polarisation and tilt angle, because both are measured under electric fields high enough to transform the TGBC* phases to the SmC* phase.

One can speculate on the structure of the TGBC phases that we denoted as TGBC*$_1$ and TGBC*$_2$. Selective reflection was detected in both TGBC* phases and not in the TGBA phase, which suggested that this reflection was connected with the helix. Also the preliminary NMR study confirmed a helicoidal smectic structure in both TGBC* phases. In (*11*), Galerne presented a model yielding a variety of TGBC* phases with commensurate order between the three characteristic parameters of the helical TGBC* phase, namely the TGB period, thickness of the smectic blocks and the helical pitch. Besides, the incommensurate phase was also possible. To describe the detailed structure, and differences between the TGBC* phases found in the materials studied, precise X-ray analysis on an oriented sample will be necessary. Detailed NMR studies in a low magnetic field will also yield information on the structural geometry of these phases (*32*).

## Acknowledgements

This work was supported by Project No. 202/05/0431 from the Czech Science Foundation and No. IAA100100710 from Grant Agency of the Academy of Sciences of the Czech Republic, Project ESF COST D35 WG13-05, Czech–Polish bilateral collaboration program No. 8 (2006–2007) and OC 175 program under the Ministry of Education, Youth and Sports of the Czech Republic. V. D. thanks the Italian PRIN2005 project and Professor C. A. Veracini for helpful discussions.

## References

(1) de Gennes P.G. *Solid State Commun.* **1972**, *10*, 753–756.
(2) Renn S.R.; Lubensky T.C. *Phys. Rev. A* **1988**, *38*, 2132–2147.
(3) Renn S.R. *Phys. Rev. A* **1992**, *45*, 953–973.
(4) Lubensky T.C.; Renn S.R. *Phys. Rev A* **1990**, *41*, 4392–4401.
(5) Goodby J.W.; Waugh M.A.; Stein S.M.; Chin E.; Pindak R.; Patel J.S. *Nature* **1989**, *337*, 449–452.
(6) Nguyen H.T.; Bouchta A.; Navailles L.; Barois P.; Isaert N.; Twieg R.T.; Maaroufi A.; Destrade C. *J. Phys. II France* **1992**, *2*, 1889–1906.
(7) Brunet M.; Navailles L.; Clark N.A. *Eur. Phys. J. E.* **2002**, *7*, 5–11.
(8) Navailles L.; Garland C.W.; Nguyen H.T. *J. Phys. II France* **1996**, *6*, 1243–1258.
(9) Ribeiro A.C.; Oswald L.; Nicoud J.F.; Soldera A.; Guillon D.; Galerne Y. *Eur. Phys. J. B* **1998**, *1*, 503–512.
(10) Lukyanchuk I. *Phys. Rev. E* **1998**, *57*, 574–581.
(11) Galerne Y. *Eur. Phys. J. E* **2000**, *3*, 355–368.
(12) Dodge M.R.; Vij J.K.; Cowling S.J.; Hall A.W.; Goodby J.W. *Liquid Crystals* **2005**, *32*, 1045–1051.
(13) Xu H.; Panarin Y.P.; Vij J.K.; Seed A.J.; Hird M.; Goodby J.W. *J. Phys.: Cond. Matter* **1995**, *7*, 7443–7452.
(14) Pandey M.B.; Dhar R.; Kuczynski W. *Ferroelectrics* **2006**, *343*, 69–82.
(15) Ismaili M.; Bougrioua F.; Isaert N.; Legrand C.; Nguyen H.T. *Phys. Rev. E* **2001**, *65*, 011701–1–15.
(16) Novotná V.; Kašpar M.; Hamplová V.; Glogarová M.; Rychetský I.; Pociecha D. *Liquid Crystals* **2004**, *31*, 1131–1141.
(17) Kašpar M.; Hamplová V.; Nov-262otná V.; Glogarová M.; Pociecha D.; Vaněk P. *Liquid Crystals* **2001**, *28*, 1203–1211.

(18) Hamplová V.; Bubnov A.; Kašpar M.; Novotná V.; Pociecha D.; Glogarová M. *Liquid Crystals* **2003**, *30*, 627–631.
(19) Hamplová V.; Bubnov A.; Kašpar M.; Novotná V.; Lhotáková Y.; Glogarová M. *Liquid Crystals* **2003**, *30*, 1463–1469.
(20) Hamplová V.; Bubnov A.; Kašpar M.; Novotná V.; Glogarová M. *Liquid Crystals* **2003**, *30*, 493–497.
(21) Hsieh W.-J.; Wu S.-L. *Mol. Cryst. Liq. Cryst.* **1997**, *302*, 253–269.
(22) Dierking I. *Textures of Liquid Crystals*; Wiley-VCH Verlag: Weinheim, 2003.
(23) Lagerwall J.P.F.; Giesselmann F.; Radcliffe M.D. *Phys. Rev. E* **2001**, *66*, 031703–1–11.
(24) Luz Z.; Meiboom S. *J. Phys. Chem.* **1963**, *39*, 366–370.
(25) Powles J.G.; Strange J.H. *Proc. Phys. Soc.* **1963**, *82*, 6–15.
(26) Catalano D.; Chiezzi L.; Domenici V.; Geppi M.; Veracini C.A. *J. Phys. Chem. B* **2003**, *107*, 10104–10113.
(27) Zhang J.; Domenici V.; Veracini C.A.; Dong R.Y. *J. Phys. Chem B* **2006**, *110*, 15193–15197.
(28) Veracini C.A. "NMR Spectra in Liquid Crystals: the Partially Averaged Spin Hamiltonian" in *"Nuclear Magnetic Resonance of Liquid Crystals"* **1985** Vol. 141, Emsley J.W. (Eds), Reidel: Dordrecht, 1985, Chapter 5, pp. p. 99.
(29) Catalano D.; Chiezzi L.; Domenici V.; Fodor-Csorba K.; Dong R.Y.; Geppi M.; Veracini C.A. *Macromol. Chem. Phys.* **2002**, *203*, 1594–1601.
(30) Catalano D.; Cifelli M.; Domenici V.; Fodor-Csorba K.; Richardson R.; Veracini C.A. *Chem. Phys. Lett.* **2001**, *346*, 259–266.
(31) Catalano D.; Domenici V.; Marini A.; Veracini C.A.; Bubnov A.; Glogarova M. *J. Phys. Chem. B* **2006**, *110*, 16459–16470.
(32) Domenici V.; Veracini C.A.; Novotná V.; Dong R.Y. *Chem. Phys. Chem.* **2008**, *9*, DOI:10.1002/cphc.200700647.
(33) Shao R.; Pang J.; Clark N.A.; Rego J.A.; Walba D.M. *Ferroelectrics* **1993**, *147*, 255–262.